# Multiple cracking of a borosilicate glass due to thermal shock

M. Dubé[a], V. Doquet[a], A Constantinescu[a]
[a] Laboratoire de Mécanique des Solides, CNRS, Ecole Polytechnique,
91128 Palaiseau cedex, France

## ABSTRACT

Continuum damage mechanics is used to model multiple cracking induced by a thermal shock in a borosilicate glass. A finite element model of the thermal shock is developed in which the elastic constitutive equations are coupled with an anisotropic stress-based damage evolution law. The Weibull distributions of strength measured in biaxial bending at various temperatures are used to identify the parameters of this damage evolution law. Vibration tests are conducted to identify the elastic properties of the glass and determine the effect of thermal shock-induced damage on the residual stiffness of the specimens, which appears to be well predicted by the model. An upper bound for the cumulated fracture surface after a thermal shock is estimated, assuming that all the elastic energy associated with the stresses above a pre-determined threshold is consumed in the creation of new surfaces. The model captures well the saturation of the crack network density for severe thermal shocks, which would not be the case without taking into account damage in the constitutive equations.

## KEYWORDS

Thermal shock, glass, cracks, continuum damage mechanics

## INTRODUCTION

Vitrification of high-activity nuclear waste for deep underground storage has become an internationally-recognized method to dispose of nuclear waste, which is first mixed with glass-forming additives, melted, poured into steel canisters and allowed to cool down naturally.

During cooling, sharp temperature gradients produce tri-axial stresses, which might induce multiple cracking. This multiple cracking is a potential issue as it would increase the area accessible to underground water during the disposal phase, once the steel over-pack has lost its water tightness. Since the amount of radionucleides which might be released in the environment depends on the effective surface of the glass block, including the surface of the crack network, the latter thus has to be evaluated.

For that purpose, various experimental methods can be used, including X-ray tomography, destructive techniques in which the canisters are cut open and the glass fragments weighted, or leaching tests. But the results issued from the various techniques are not fully consistent.

This study shows how an upper bound of the cumulated fracture surface can be estimated by thermo-mechanical finite element simulations, assuming that the elastic energy associated with the transient tensile stresses is fully converted into surface energy and using an anisotropic damage evolution law coupled with thermo-elastic constitutive equations.

## GLASS CONSTITUTIVE EQUATIONS

At temperatures approaching the glass transition temperature of 502℃, the SON 68 borosilicate glass exhibits a visco-elastic behavior. Relaxation tests were conducted to characterize this behavior; however, since the present work focuses on low temperatures (T < 200℃) and short term experiments, the viscosity can be neglected.

Continuum damage mechanics is suitable to describe the stiffness degradation of a material undergoing damage, especially for brittle materials. A simple anisotropic damage model was developed by Sun & Khaleel [1]. Though the original model was meant to take into account the effect of shear stresses, only the diagonal terms of the damage tensor, i.e., damage due to tensile principal stresses was accounted for in this study.

The stiffness degradation arising from the damage accumulation was simulated by adding a damage tensor into the glass constitutive equation:

$$\sigma_{ij} = \left\{ K^e_{ijkl}(T) + K^d_{ijkl}(T) \right\} \cdot \left\{ \varepsilon_{kl} - \varepsilon^{th}_{kl} \right\} \tag{1}$$

in which $K^e_{ijkl}(T)$ and $K^d_{ijkl}(T)$ are the temperature-dependent fourth order stiffness tensors representing the undamaged isotropic material and the added influence of damage, respectively. $\varepsilon^{th}$ stands for the thermal strain tensor. The stiffness tensors are given by:

$$\mathrm{K}^{\mathrm{e}}_{\mathrm{ijkl}} = \lambda(T)\delta_{ij}\delta_{kl} + \mu(T)\left(\delta_{ik}\delta_{jl} + \delta_{il}\delta_{kj}\right) \tag{2}$$

$$\mathrm{K}^{\mathrm{d}}_{\mathrm{ijkl}} = C_1(T)\left(\delta_{ij}D_{kl} + \delta_{kl}D_{ij}\right) + C_2(T)\left(\delta_{jk}D_{il} + \delta_{il}D_{jk}\right) \tag{3}$$

where *λ(T)* and *μ(T)* are Lame's coefficients, $D_{ij}$ are the damage parameters and $C_1(T)$ and $C_2(T)$ are temperature-dependent coefficients. The terms of the damage tensor, $D_{ij}$, take values between zero and one, the latter meaning that the material is fully damaged and can no longer sustain stresses. They are assumed to follow a linear evolution law:

$$D_{ii} = \begin{cases} 0 & \sigma_i \leq \sigma_{th} \\ \dfrac{\sigma_i - \sigma_{th}(T)}{\sigma_c(T) - \sigma_{th}(T)}, & \sigma_{th} < \sigma_i < \sigma_c \\ 1 & \sigma_i \geq \sigma_c \end{cases} \tag{4}$$

where $i$ = 1, 2, 3, $\sigma_i$ is the $i^{th}$ principal tensile stress, $\sigma_{th}(T)$ is the temperature-dependent threshold stress under which no damage occurs and $\sigma_c(T)$ is the critical stress above which the material is fully damaged.

$C_1$ and $C_2$ were identified by stating that the axial stress $\sigma_{11}$ is zero when $D_{11}$ = 1.0, for a tension test in direction 1, i.e., for $D_{22} = D_{33} = 0$ [1]. Following this logic, we find $C_1 = \mu$ and $C_2 = -1.5\mu$. Note that in the application considered below (thin disk specimens subjected to a thermal shock) loading is proportional, so that the principal axes do not change with time and correspond to the radial, tangential and normal directions. The damage tensor will thus be naturally defined in this coordinate system.

## IDENTIFICATION OF THE PARAMETERS FOR THERMO-MECHANICAL MODELLING

The heat capacity of the glass was determined by differential scanning calorimetry and the diffusivity by the laser flash method. The thermal expansion coefficient $\alpha$ was determined by dilatometry and the thermal conductivity was deduced.
The threshold and critical stresses in equation 4 were identified using biaxial flexural tests carried out according to the ASTM C 1499 – 05 standard test method [2], on 2mm-thick disk specimens with a diameter of 40mm, polished to a roughness of 1µm. The disks were placed between a 30 mm diameter support ring and a 10 mm diameter concentric loading ring. Displacement-controlled monotonic loading was applied on the loading ring until failure.

17 to 20 specimens were tested at 20, 200 and 506°C in order to have a minimum of 13 valid tests at each temperature. Tests were considered valid when the fracture origin was located inside the diameter of the smaller loading ring where uniform equibiaxial tension prevails. Optical microscopy revealed that bubbles, as large as 1mm, responsible for residual stresses and stress concentration acted as initiation sites.

The measured cumulative strength distributions are plotted on Fig. 1. The strength of the glass appeared not to vary significantly within the investigated temperature range. The Weibull modulus was around 6. The threshold stress for damage, $\sigma_{th}$, was determined as the lowest strength obtained during the tests, i.e. 41 MPa. Based on the recommendations of Sun & Khaleel [1], the average of all measured strengths, corresponding to 64 MPa, was selected as the critical stress, $\sigma_c$, independent of T, as well. The force-displacement data recorded during the tests were used to obtain the elastic properties of the glass. The Young's modulus for a circular plate under biaxial flexural loading can be estimated from:

$$E \cong \frac{3F\left(1-\upsilon^2\right)d_l^2}{8\pi\delta h^3}\left(\frac{d_s^2}{d_l^2}\left[1+\frac{(1-\upsilon)\left(d_s^2-d_l^2\right)}{2(1+\upsilon)d_d^2}\right]-\left(1+\ln\frac{d_s}{d_l}\right)\right) \tag{5}$$

In which $\delta$ is the deflection [2]. A first relationship between Young's modulus and Poisson's ratio is obtained with this equation but a second test is needed to identify the two properties separately.

For that purpose, measurements of modal frequencies during vibration tests on disk specimens were performed between room temperature and 506°C thanks to a radiant oven. The specimens supported by rubber bands bonded on their outer surface and attached to a metallic structure were excited by a hammer and their acoustic response was captured by a microphone connected to an amplifier and an oscillator. A Fourier transform was applied on the signal in order to obtain the first and second modal frequencies. According to Fletcher & Rossing [3], the relation between the first modal frequency and the elastic constants of a thin disk of radius R is:

$$\mathrm{f}_0 = \sqrt{\frac{\mathrm{E}}{\rho\left(1-\upsilon^2\right)}}\frac{\mathrm{h}}{\mathrm{R}^2}\beta \tag{6}$$

In which $\beta$ is a boundary conditions-dependent coefficient that takes a value of 0.2413 for free edges [3].
Equations 5 and 6 provide two independent relations from which the Young's modulus and Poisson's ratio at 20, 100, 200, 300, 400 and 500°C were computed. A linear interpolation was done for intermediate temperatures. Lamé's coefficients in equation 2 were then deduced, assuming isotropy of the undamaged glass.

## THERMAL SHOCK DAMAGE

Thermal shock experiments were carried out on 2mm-thick disk specimens heated to a pre-determined temperature in a radiant oven then quenched into water kept at room temperature. The specimens were then observed by optical microscopy in order to assess the thermal shock-induced damage. Approximately 20 micrographs were taken for each specimen. The observations revealed many curved and branched cracks. This curvature can be explained by (i) the equibiaxial tensile stress field which arises during the thermal shock and (ii) the mode-mixity induced by the interactions between cracks.

The cumulated developed length of cracks on both the upper and lower surfaces, denoted by $l_c$, was determined from these micrographs, taking the curvature into account. In order to measure the depth of the cracks, several specimens were cut along different diameters. The cracks were curved in that plane as well, due to mutual interactions which increase with the severity of the thermal shock and the density of the crack network. The average developed "depth" of cracks on those transverse sections, denoted by $d_c$, was measured. The cumulated fractured surface was finally approximated as:

$$S_{tot} = l_c d_c \tag{7}$$

An axial-symmetric thermo-mechanical finite element model of the thermal shock was developed. The cross section of the disks was meshed with eight-node quadratic elements. 18 and 40 elements were used across the thickness and radius of the disk, respectively. Convection boundary conditions were applied on the free surfaces. A convection heat transfer coefficient h = 10,000 W/m$^2$/℃ was used, in accordance with the literature. Th e thermal stresses were computed based on the anisotropic damage evolution law presented above. The stresses were computed at each step, n, as:

$$\sigma_{ij}^{n} = \left\{ K_{ijkl}^{e} + K_{ijkl}^{d,(n-1)} \right\} \cdot \left\{ \varepsilon_{kl}^{n} - \varepsilon_{kl}^{th,n} \right\} \tag{8}$$

Convergence in terms of mesh refinement and time increment was checked.

Upon cooling, tensile stresses are generated on the outer surfaces of the disks. The state of stress is equibiaxial with $\sigma_{rr} = \sigma_{\theta\theta}$ and $\sigma_{zz} = 0$, corresponding to the principal stresses. The evolution of these stresses with time is depicted on Figure  for a point located at mid-radius, on the outer surface of the specimen, for a thermal shock amplitude ΔT = 157℃. The curve obtained using thermo-elastic constitutive equations without damage is also plotted for comparison. When accounting for damage, the stresses are cut off at the critical stress $\sigma_c$ = 64MPa, whereas they reach 88MPa, which is above the maximum of the strength distribution plotted on Figure , if damage is not taken into account. As expected, $\sigma_{rr}$ and $\sigma_{\theta\theta}$ are positive on the outer surfaces of the disk and becomes negative at a certain depth.
Figure  shows the profile of the damage parameter $D_{11}$ along a transverse section after thermal shocks of various amplitudes. As in the experiments, two superficial damaged layers appear. The larger ΔT, the deeper the damage penetrates inside the specimens.

One of the objectives of the study is to estimate the cumulated fracture surface in a glass specimen subjected to a thermal shock. An upper bound was obtained by stating that that all the elastic energy associated with the transient stresses above the threshold stress is consumed in the creation of new surfaces. The peak value of the elastic energy over the time was computed as:

$$Max_{time} \frac{1}{2} \int_{V_{\sigma \geq \sigma_{th}}} \sigma_{ij} \varepsilon_{ij} dV \approx 2\gamma_s S_{tot} \tag{9}$$

In which $V_{\sigma \geq \sigma th}$ is the volume over which the threshold stress is reached by at least one principal stress, $S_{tot}$ ($m^2$) is the total fractured surface and $\gamma_s$ ($J/m^2$) is the surface energy which is determined by:

$$\gamma_s = \frac{\left(1-\nu^2\right)K_{Ic}^2}{2E} \qquad (10)$$

in which $K_{Ic}$ is the material toughness, 0.85MPa√m, measured on DCDC specimens at room temperature and assumed to remain constant up to 200℃.

The measured and predicted fractured surfaces are compared on Figure  for various thermal shock amplitudes. The fractured surface predicted by a standard thermo-mechanical model that does not account for damage is also shown as a reference. At low thermal shock amplitudes, a fairly accurate prediction is obtained for both models.

By contrast, at high thermal shock amplitudes, i.e., $\Delta T \geq 157℃$, the model that does not account for damage does not predict the saturation of the fractured surface. This result was expected as the stresses, and therefore the computed elastic energy, should keep increasing with the thermal shock amplitude. The model accounting for damage succeeds in predicting the saturation of the fractured area at $\Delta T \geq 157℃$. Though the model somewhat overestimates the fractured surface, it provides an upper bound of the fractured area. It is assumed that the excess elastic energy, i.e., the part that is not dissipated into the creation of new surfaces, is dissipated into other forms such as vibrations, acoustic energy, etc. Some error on the convection heat transfer coefficient, h, might also partly explain the discrepancy.

The reduction in stiffness of the specimens due to thermal shock-induced damage was assessed by measuring the modal frequencies of pre-damaged specimens at room temperature. Due to the damage-induced anisotropy and heterogeneity of the specimens after the thermal shocks, their elasticity cannot be expressed in terms of Young's modulus and Poisson's ratio. The ratio of modal frequencies measured after and before the thermal shock provides a global and more pertinent evaluation of the stiffness reduction and is plotted on Figure 5.
This ratio can also be estimated by numerical simulations. An axial-symmetric finite element model of the vibration test was developed based on the same mesh as that used for the thermal shock simulation starting with the final stiffness tensor obtained at the end of thermal shock simulation, i.e., $K_{ijkl}^{e} + K_{ijkl}^{d\ N}$. The stiffness reduction predicted by finite element is compared to that obtained from experiments on Fig. 5. It follows the same trend as that measured experimentally with the predicted values falling within the experimental error bars.

Following the thermal shocks, the disks were broken in biaxial bending in order to measure their residual strength. A sharp drop in strength is observed for an amplitude $\Delta T_c \approx 77℃$, above which it remains nearly constant, in accordance with Hasselman's observations [4].

Pre-damaged specimens revealed a different failure behavior from that observed for the virgin specimens. As shown on figure 6b, the cracks followed an irregular path due to further extension and coalescence of several pre-existing cracks generated by the thermal shock. This contrasts with the straighter crack paths observed for the undamaged material (fig. 6a) which failed by extension of a single crack that initiated near the center of the disk and then branched and propagated along more or less radial directions.
The damage model cannot be applied as such to predict the residual strength of damaged specimens in biaxial bending. Indeed, numerical difficulties (mesh dependency, non convergence close to final fracture, etc.) that are quite common with such a local model

would be encountered [5]. A non-local formulation of the model should be developed in the future, allowing for these difficulties to be overcome and the residual strength to be predicted.

## CONCLUSIONS

The thermo-mechanical behavior of a borosilicate glass used for nuclear waste vitrification was investigated by experiments and numerical simulations. A continuum damage mechanics model was identified and used to predict the damage induced by a thermal shock. Comparison between predicted and measured damage based on the residual stiffness of the glass was performed, and a satisfactory agreement was obtained. An upper bound of the total fractured surface induced during a thermal shock was estimated, assuming that the elastic energy associated to the transient stresses that are higher than a threshold value is dissipated in the creation of new surfaces. The damage model captured the saturation of the crack network density for severe thermal shocks.

## ACKNOWLEDGEMENTS

The authors are indebted to Frédéric Bouyer from the CEA for providing the SON 68 glass and Xavier Boutillon from LMS for valuable advices regarding vibrational measurements. The CEA, Andra and AREVA are also gratefully acknowledged for supporting this study.

## REFERENCES

[1] Sun X, Khaleel M.A. (2004). Modeling of Glass Fracture Damage Using Continuum Damage Mechanics . International Journal of Damage Mechanics, 13, 263-284.
[2] ASTM C 1499 – 05 (2005). Standard Test Method for Monotonic Equibiaxial Flexural Strength of Advanced Ceramics at Ambiant Temperature. ASTM International.
[3] Fletcher N.H, Rossing T.D. (1998). The Physics of Musical Instruments, Springer Science + Business Media Inc.
[4] Hasselman D.P.H. (1969). Unified Theory of Thermal Shock Fracture Initiation and Crack Propagation in Brittle Ceramics. Journal of American Ceramic Society, 52, 11, 600-604.
[5] Lemaitre J, Chaboche J.L, Benallal A, Desmorat R, (2009). Mécanique des Matériaux Solides, 3rd edition, Dunod, Paris.

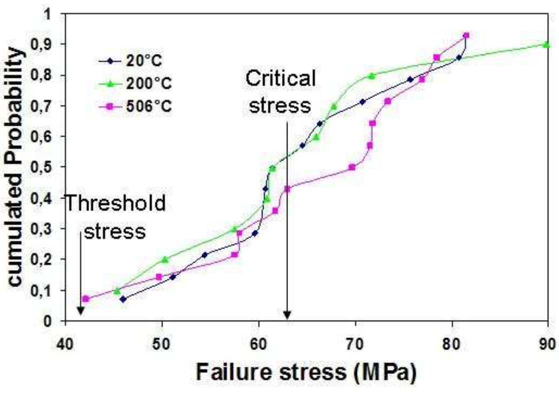


Figure 1: Biaxial flexural strength distributions of SON 68 glass at various temperatures

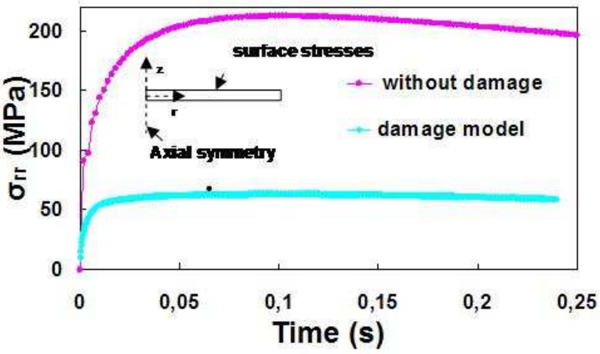


Figure 2: Time evolution of surface stresses during a thermal shock of amplitude ΔT = 157℃

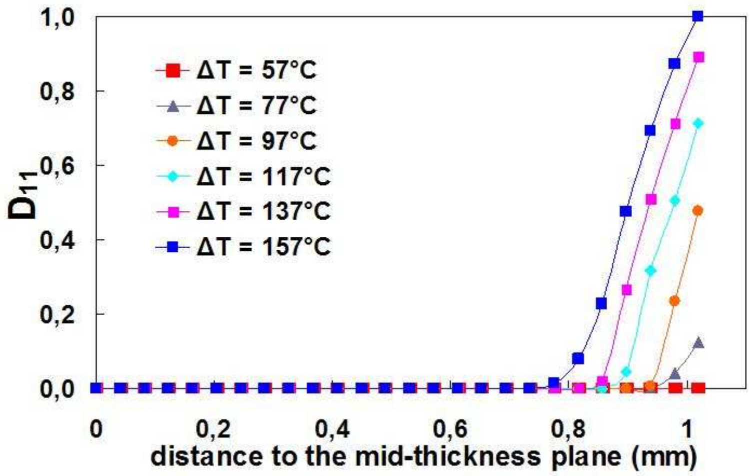


Figure 3: Profiles of $D_{11}$ along a transverse section after thermal shocks of amplitudes ΔT.

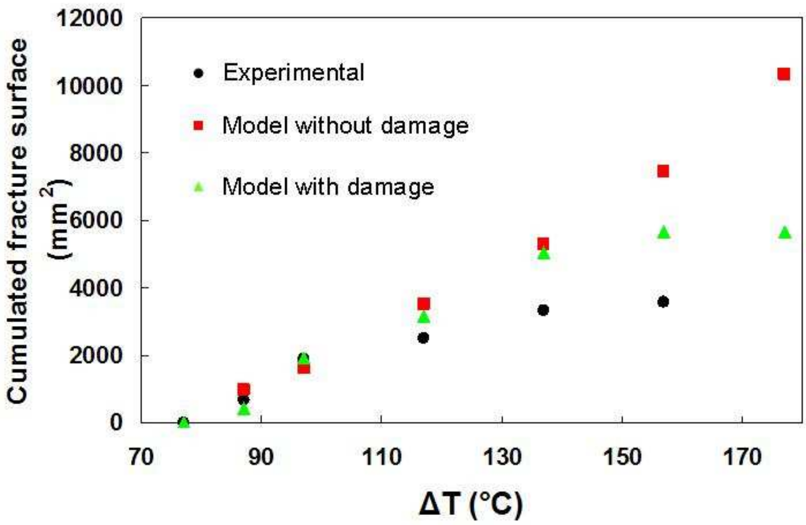


Figure 4: Predicted and measured cumulated fracture surfaces due to thermal shocks

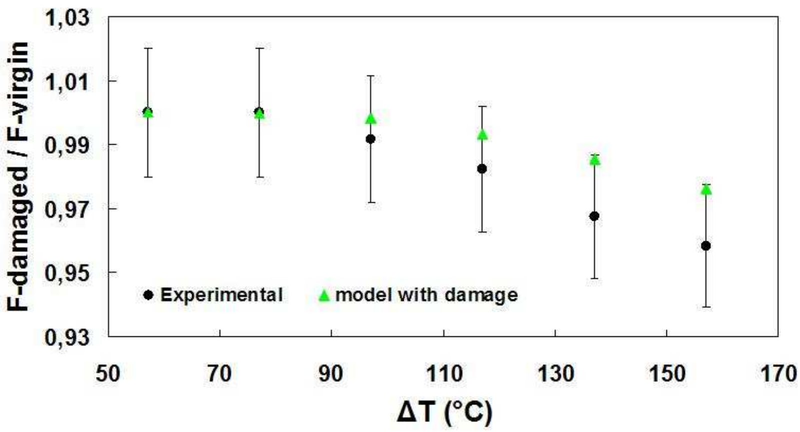


Figure 5: Computed and measured natural frequencies of damaged specimens

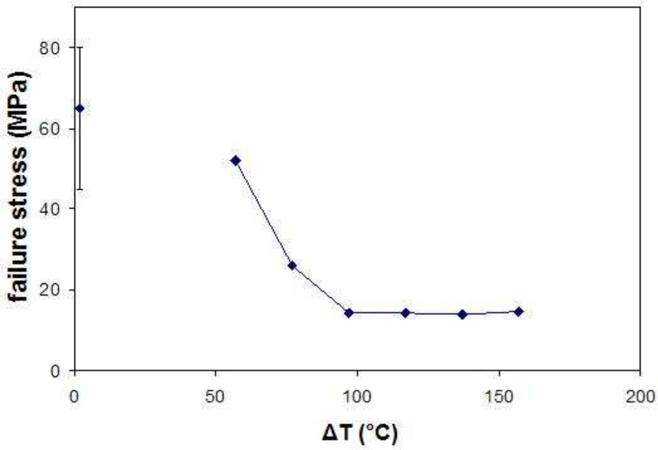


Figure 6: Residual biaxial flexural strength after thermal shocks of amplitudes ΔT

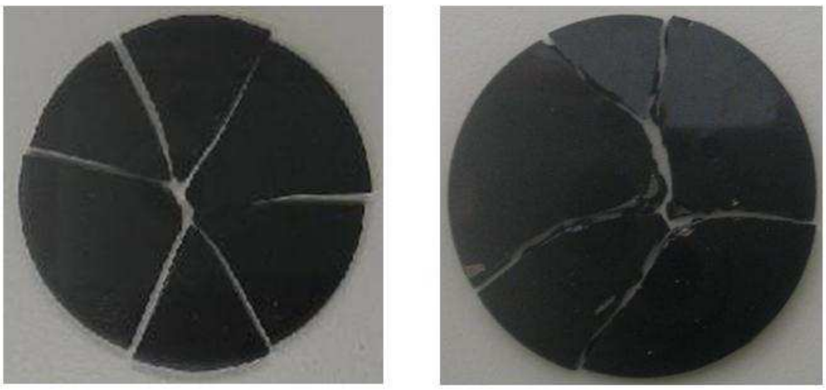

Figure 7: Glass disks fractured in biaxial bending a) virgin disk b) after a thermal shock

**Corresponding author:** doquet@lms.polytechnique.fr